Use of Low-order Simulations to Predict Proximity Interactions in Traffic

Faegheh Ghorbanishohrat, Brian R. McAuliffe

National Research Council Canada
1200 Montreal Rd., Ottawa, Ontario, Canada, K1A 0R6

Faegheh.Ghorbanishohrat@nrc-cnrc.gc.ca
Brian.McAuliffe@ nrc-cnrc.gc.ca

Abstract: The aerodynamic performance of road vehicles is quantified conventionally via isolated-vehicle assumptions, while recent research has shown that aerodynamic forces and moments can vary by +/-50% in traffic, associated with proximity to vehicles in adjacent lanes. Mapping the aerodynamic performance for common traffic scenarios requires hours of wind tunnel testing or time-consuming road measurements. These interactions are caused predominantly by pressure field interactions and blockage effects, which can be replicated reasonably well using low-order CFD modelling. This paper examines various levels of simplification, including coarse-mesh simulations using a commercial CFD solver and a potential-flow method, to predict the proximity interactions observed in experimental wind-tunnel results.

1 Background and Objectives

Aerodynamic interactions between road vehicles in traffic has emerged in recent years as a topic of interest, related to energy-use and emissions from transportation systems and to vehicle autonomy via platooning concepts [1,2]. Two distinct phenomena dominate these interactions.

Wakes from surrounding vehicles introduce flow-field variations that can reduce the aerodynamic drag of a following vehicle, due to the lower effective wind speed [3], or can momentarily increase the drag when impinging from vehicles in opposing traffic [4]. These wake effects can persist for large distances from the wake-source vehicle, up to hundreds of meters [5].

In close proximity (within a vehicle dimension), pressure fields interact to generate significant increases or decreases in aerodynamic forces and moments, relative to isolated-vehicle conditions [6]. Most notably, in a close-longitudinal-following configuration (i.e. platoon configuration), the pressure field forward of a trailing vehicle interacts with the body and wake region of a leading vehicle to increase the

Contribution: 2025 FKFS Conference on Vehicle Aerodynamics and Thermal Management
15 – 16 October 2025 | Leinfelden-Echterdingen

base pressure of the leading vehicle and reduce its drag. Interactions amongst vehicles in adjacent lanes also lead to significant increases or decreases in aerodynamic forces and moments [7]. Based on the authors' previous work [8], these proximity effects appear to be dominated by interacting blockage effects on the surrounding flow field, leading to a hypothesis that these influences can be predicted by low-order computational methods. Blockage corrections for wind tunnels have been successfully developed based on potential-flow theory [9], suggesting similar methods may be suitable for proximity interactions. Low-order computational-fluid-dynamics (CFD) methods, such as panel methods or coarse-grid Reynolds-averaged Navier-Stokes (RANS) methods, may also provide efficient techniques to predict these influences.

The objective of this paper is to examine two simulation approaches to predicting proximity interactions for vehicles travelling in adjacent lanes. One approach uses a coarse-grid RANS method for a two-vehicle system, described in Section 2. The other approach uses a simple potential-flow method that combines source and sink models with a uniform flow to represent a multi-vehicle system, described in Section 3. Wind conditions for this preliminary study are limited to 0° yaw angle.

Results from the two methods are contrasted with wind-tunnel measurements of a two-vehicle combination (sedan + SUV), using incremental drag-coefficient and surface-pressure-coefficient values as indicators of their suitability. The measurements were conducted at 15% scale in the NRC 2 m x 3 m Wind Tunnel using a DrivAer Notchback model and an AeroSUV Estateback model [8]. The data provide measurements for a range of longitudinal distances (±2 vehicle lengths) for a lateral separation representing a typical North American highway lane width (3.7 m full scale, providing approximately one vehicle-width separation). Measurements demonstrated drag-coefficient reductions for the individual vehicles up to about 10% and increases that exceeded 20%.

2 Reynolds-Averaged Navier-Stokes Method

2.1 Geometric Model and Computational Domain

For this study, CFD analysis was performed on a full-scale, simplified mid-sized SUV model (L×W×H: 4764 mm ×1936 mm ×1700 mm). The simulations were designed to analyze the aerodynamic interaction between two identical SUV models traveling in adjacent lanes. The vehicles were configured with a constant lateral, centre to centre separation of 3.7 m, a value corresponding to the average width of a common road lane. The primary variable was the longitudinal spacing between the vehicles, defined relative to the vehicle length (L). A matrix of five test cases was studied corresponding to longitudinal separation distances (x) of x/L=0, 0.5, 1.0, 1.5, and 2.0.

The domain is illustrated in Figure 1, which extends approximately 5.5 vehicle lengths (L) upstream, 10.5 lengths downstream, 16 vehicle widths (W) across, and 12 vehicle

heights (H) vertically from the primary vehicle. This configuration yields frontal area blockage ratios of 0.5% for the isolated vehicle case and 1% for the proximity configurations, both of which are well within the acceptable limits for bluff body aerodynamic simulations.

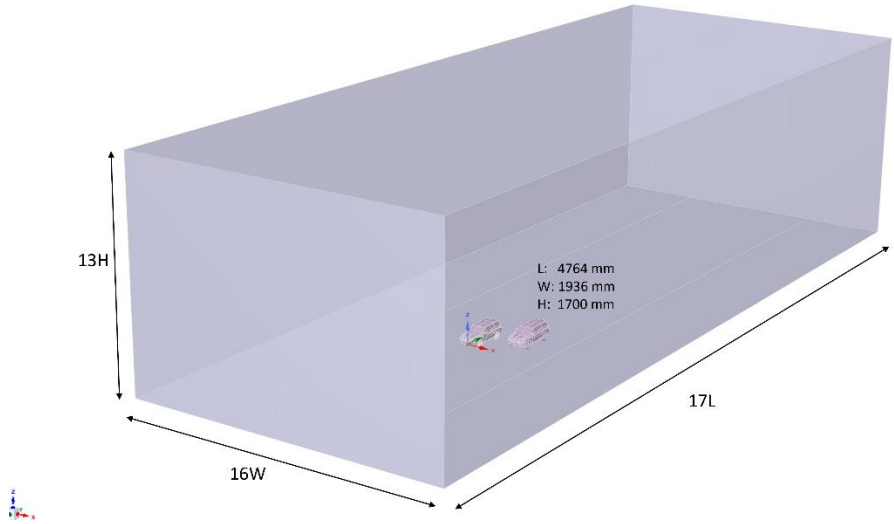

Figure 1: Schematic of the full-scale computational domain and vehicle models.

2.2 Numerical Simulation Setup

All simulations were performed using the commercial software package ANSYS Fluent. The analysis employed a steady-state Reynolds-Averaged Navier-Stokes (RANS) approach to solve the governing equations of fluid flow. Turbulence effects were modeled using the k-ω Shear Stress Transport (SST) model [10]. The simulation was configured with an inlet velocity of 29 m/s (~105 km/h) at a 0° yaw angle. To model the road interface, a moving ground boundary condition was applied at the same velocity as the inlet flow. For computational simplification, the wheels were modeled as stationary.

2.3 Meshing and Grid Independence

The domain was discretized using a poly-hexcore mesh, which employs a combination of polyhedral and hexagonal cells to efficiently capture complex geometry. To ensure computational accuracy, multiple bodies of influence were implemented to selectively refine the mesh density in regions with significant flow gradients.

A grid sensitivity analysis was performed to ensure the numerical results of interest were independent of mesh resolution. Four distinct mesh densities were evaluated for an isolated vehicle and a two-vehicle proximity configuration, with the convergence of the drag coefficient (C_D) Presented in Table 1. The primary objective of this study is to predict the change in aerodynamic drag resulting from vehicle proximity in traffic situations. Consequently, the key metric is the delta drag coefficient (ΔC_D), rather than the absolute C_D value. Table 2 summarizes this metric, showing the change in drag for each vehicle in a specific proximity case relative to its isolated baseline. This configuration—with the proximity vehicle positioned one lane-width away laterally and half a vehicle length behind the primary model—was selected for detailed analysis as it has been identified in previous research [8] to produce the maximum changes in drag for the individual vehicles (increase for lead vehicle, decrease for trailing vehicle).

To ensure a margin of safety for numerical accuracy, the mesh selected for the rest of simulations was the second coarsest. The final mesh consists of approximately 10.8 million cells for the isolated vehicle simulation and 19 million cells for the two-vehicle proximity case. Fine-scale refinement was applied in high-curvature regions of the vehicle model, achieving a minimum face area of 3.5×10^{-3} mm² and a minimum cell volume of 3.9×10^{-3} mm³.

The grid sensitivity analysis (Table 1) showed a total variation of 2-3% in the drag coefficient (C_D) across all tested meshes. Critically, the variation between the 8 million cell and 18 million cell grids was less than 1%. This demonstrated that a grid-independent solution was reasonably achieved. The 10.8 million cell mesh was deemed sufficient for the study's primary objective of estimating the delta drag coefficient relative to isolated vehicle (ΔC_D), which is in range of 4%-20%.

Table1: Drag coefficient (C_D) of a simplified mid-sized SUV model for the isolated and proximity vehicle cases for various meshes.

Isolated vehicle Mesh	Proximity Model Mesh	C_D Isolated	C_D Leading vehicle	C_D Following Vehicle
57,519,272	98,535,909	0.301	0.354	0.272
17,535,439	29,514,219	0.306	0.359	0.279
10,775,254	19,215,304	0.305	0.358	0.28
7,973,372	13,802,265	0.306	0.362	0.28

Table2: ΔC_D for the isolated and proximity vehicle cases for various meshes.

Proximity Model Mesh	C_D System	ΔC_D Lead-Follow	ΔC_D Isolated-Lead	ΔC_D Isolated-Follow	ΔC_D Isolated-System
98,535,909	0.313	0.082	0.053	-0.029	0.012
29,514,219	0.319	0.080	0.053	-0.027	0.013
19,215,304	0.319	0.078	0.053	-0.025	0.014
13,802,265	0.321	0.082	0.056	-0.026	0.015

2.4 Results of Proximity Influence

Figure 2 illustrates the drag coefficient (C_D) and delta drag coefficient (ΔC_D) for all tested configurations from x/L=0 to 2.0. The most significant aerodynamic interaction occurs at a longitudinal separation of x/L=0.5. At this critical spacing, the primary model experiences an 18% drag increase, while the proximity model benefits from an 8% drag reduction. Although the experimental data of [8] uses vehicles of different shapes and sizes, these ΔC_D values align well with the magnitudes observed in the wind-tunnel study, on the order of 20% increase for the leading vehicle and 10% decrease for the trailing vehicle. The net effect on the two-vehicle system is a drag penalty of approximately 5%. The analysis further reveals the sensitivity of these interactions, with the lead model's performance ranging from the 18% drag increase at x/L=0.5 to 4% drag decrease at x/L=2.0.

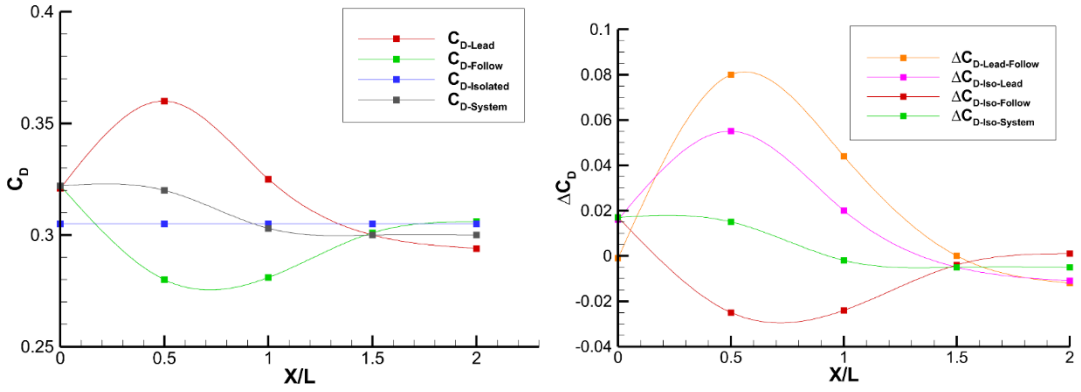

Figure 2: CD and ΔCD for the isolated and proximity vehicle cases at various longitudinal separations (x/L=0,0.5,1.0,1.5, and 2.0).

Figure 3 presents the static pressure contours on the vehicle surfaces and on a horizontal plane 0.25 m above the ground, comparing the isolated vehicle against the x/L=0.5 and x/L=2.0 proximity configurations. The figure visually confirms the aerodynamic coupling between the vehicles, with a lower C_P between the vehicle in the middle plot identifying the mutual blockage influence between the two bodies.

It is important, however, to contextualize these findings within the known limitations of the steady-state RANS methodology. A recent study by Aultman et al. [11] investigated various simulation methods (RANS, URANS, DDES) for automotive aerodynamics. Their findings showed that while RANS can provide fairly accurate predictions of the overall drag coefficient, it often fails to accurately capture detailed flow features. Specifically, they noted that RANS modeled the flow poorly in the vehicle's wake, yielding a structure inconsistent with unsteady simulations and experiments. Aultman et al. attribute this discrepancy to the RANS model's tendency to predict larger regions of flow separation, leading to an over-prediction of base drag.

The primary objective of this study is to quantify the aerodynamic proximity effect, rather than to obtain a perfectly resolved flow field. If the presence of a second vehicle primarily alters existing flow parameters without inducing new, large-scale phenomena like flow separation, then analyzing the difference between isolated and proximity cases with RANS may provide an estimation of system drag. This assumption is supported by the cumulative drag coefficient data versus the distance along the vehicle length (x_v) in Figure 4, which shows similar trends between the multi-vehicle cases and the isolated-vehicle case. These drag-accumulation plots show that, for x/L=0.5, the lead vehicle experiences drag increase from a mid-length position (around x_v/L=0.3) and a significant increase at its base, while the trailing vehicle experiences its drag reduction over its forward section (forward of about x_v/L=0.4).

The results provide evidence for this approach. At the largest tested separation of x/L=2.0, the pressure distribution on the trailing vehicle closely mirrors that of the isolated case, consistent with their nearly identical C_D values. Despite this large separation between the vehicles, a discernible interference effect persists: the presence of the trailing vehicle modifies the pressure field in the wake of the lead vehicle, resulting in a drag reduction of approximately 3% for the leading vehicle.

It is acknowledged that the RANS model does not replicate perfectly the true physical flow, particularly in regions of complex turbulence and separation. However, if the RANS method can accurately capture the relative change in the pressure field induced by vehicle proximity, it serves as a highly efficient tool for estimating these effects, offering substantial savings in computational time. Further investigation, with mesh densities for different vehicle-size and vehicle-shape combinations, and comparison against corresponding experimental data, is required to validate this hypothesis.

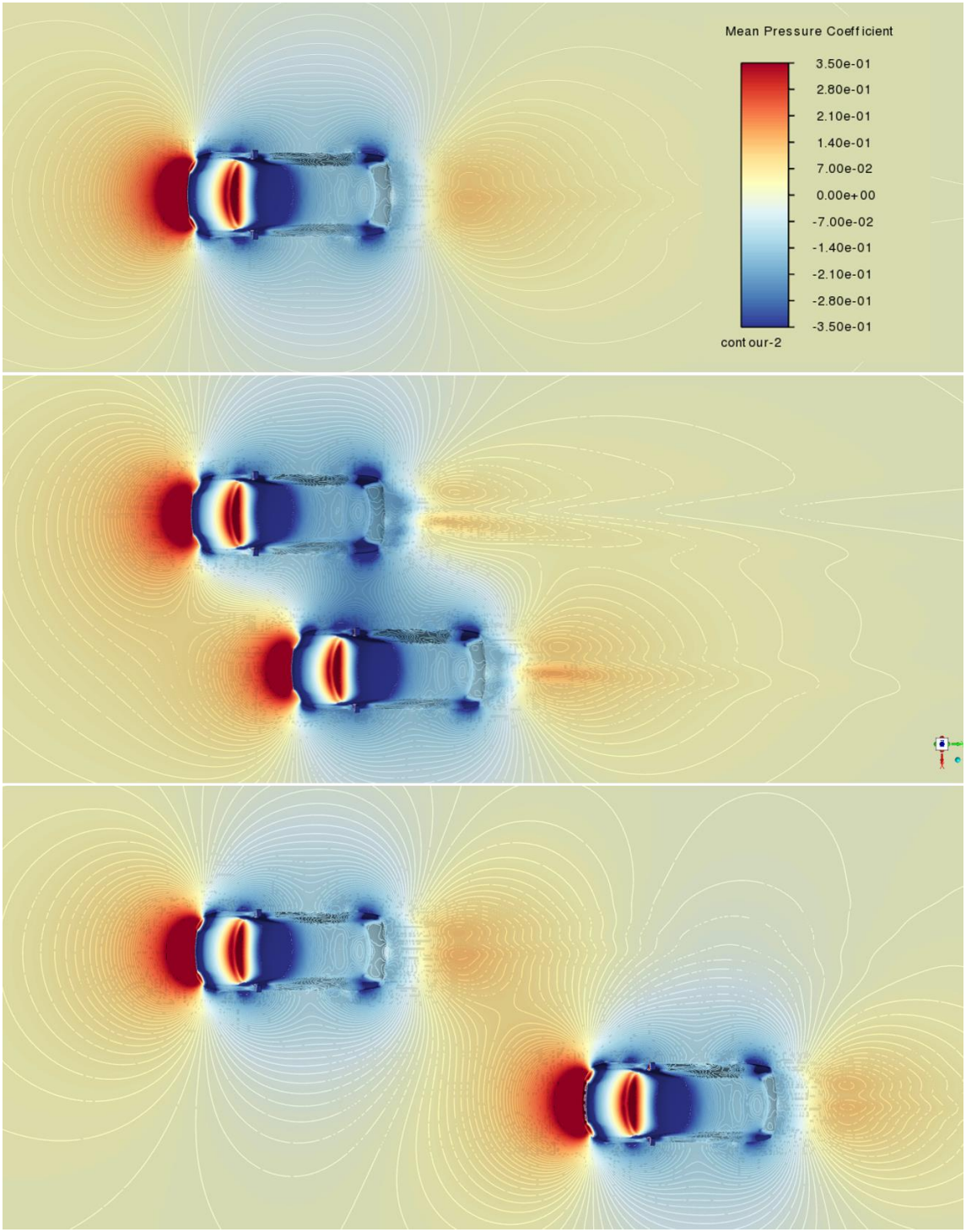

Figure 3: Mean pressure coefficient for Isolated, x/L=0.5 and x/L=2 simulations (from top to bottom) on vehicle's surface and a surface of the plane located at 0.25 m above the ground.

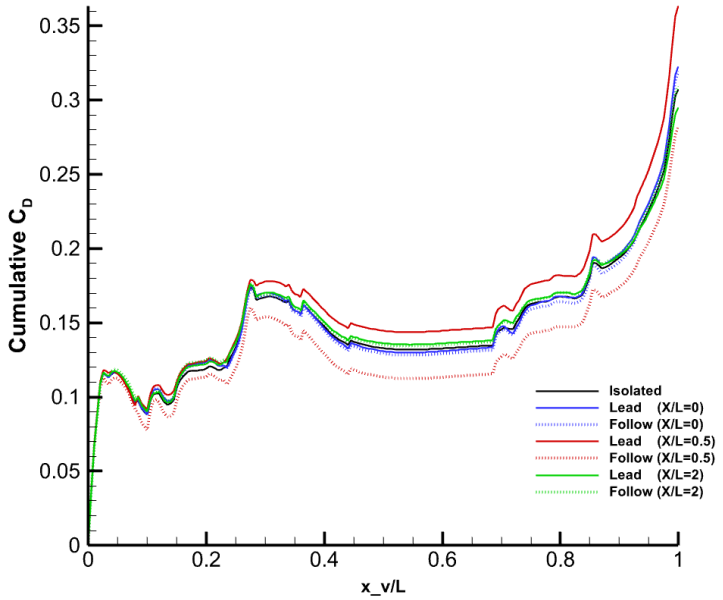

Figure 4: Drag accumulation graph for Isolated, and two proximity models simulations.

3 Potential Flow Method

A three-dimensional potential-flow method has been adopted for this investigation. This method is based on the superposition of potential flows associated with sources/sinks pairs placed strategically to represent solid-body disturbances associated with each vehicle, and sources placed appropriately to generate a wake disturbance for each vehicle. The sources and sinks are placed on the ground plane such that the symmetry about this plane represents the solid ground. This follows the approaches used for wind-tunnel blockage corrections [9], whereby a three-dimensional doublet is generally used to represent the solid blockage of a body in a duplex-tunnel arrangement. Here, the use of a source/sink pair, instead of a doublet, provides a disturbance representative of an ellipsoid rather than a sphere, mimicking better the longitudinal spatial extent of a road vehicle.

The induced velocity of a source is defined as

$$u_i = \frac{S}{4\pi}\left(\frac{x_i}{(x_1^2 + x_2^2 + x_3^2)^{3/2}}\right) \tag{1}$$

where *i* represents the coordinate direction (1,2,3 representing x,y,z directions), and S is the strength of the source (+ for sources, - for sinks). These induced velocities, for N sources and/or sinks, are superimposed on the freestream flow, $U = [U_{fs},0,0]$, to define the flow field:

$$u_i = U_i + \sum_{n=0}^{N} u_{i,n} \tag{2}$$

The source/sink strengths are modelled after the formulation often used for the wake source [9], related to the drag of the vehicle:

$$S_{wake} = \frac{1}{2} C_D A_F U_{fs} \tag{3}$$

Here, this formulation is applied to the source/sink pairs for each vehicle body, with a scaling factor, Θ_{body}, to provide the large disturbances of the body while providing an approximate way to scale for different vehicle sizes. The magnitude of S_{wake} from Equation 3, although adequate for blockage correction methods that represent effects on the bulk flow in a test section, may be inadequate to provide the localized effect of wake displacement in close proximity to another vehicle. As such, a scaling factor Θ_{wake} is also applied to the wake source strength.

The relative positions of the source-sink pairs for the body displacement and the sources for the wake displacement are an important consideration for the proximity-effects analysis. Comparisons of CFD velocity flow fields to those produced by a potential-flow method permitted reasonable estimation of the source/sink locations to simulate the flow displacement around a road-vehicle shape.

The incremental changes to the drag of each vehicle were evaluated based on changes to the pressure field around each body. Based on the calculated velocity field, the pressure-coefficient field is calculated as:

$$C_P = 1 - \left(\frac{U}{U_{fs}}\right)^2 = 1 - \frac{u_1^2 + u_2^2 + u_3^2}{U_{fs}^2} \tag{4}$$

For each vehicle of the multi-body simulation, changes to the pressure-coefficient field are then calculated as:

$$\Delta C_{P,v} = C_P - C_{P,v,iso} \tag{5}$$

where *v* represents each individual vehicle and *iso* refers to the calculated isolated-vehicle pressure field. The non-linear nature of the pressure, compared to the linearly-superimposed velocity field, results in a non-zero ΔC_P field for each vehicle that represents localized changes to the static pressure associated with proximity to another vehicle.

A validation of this potential-flow approach is provided in Figure 5, comparing an estimate of the potential-flow solution for ΔC_P with experimental measurements for the two vehicles on which the calculations are based, those being a DrivAer Notchback (DN) and AeroSUV Estateback (SE) [8]. The results for the potential-flow solution are based on an interpolation of the ΔC_P fields for each assumed vehicle to the spatial locations of the pressure taps on the wind-tunnel models. The general ΔC_P patterns and magnitudes match well and highlight, for this case with a half-vehicle-length offset, the concentration of significant negative incremental pressure near the physical centre of the two-body system, resulting from the mutually-combined blockage effect. Additionally, the potential method captures well the pressure increase on the forward right side (from a driver perspective) of the lead AeroSUV body, and captures the greater incremental negative ΔC_P on the left side of the DrivAer body, due to the influence of the larger AeroSUV model.

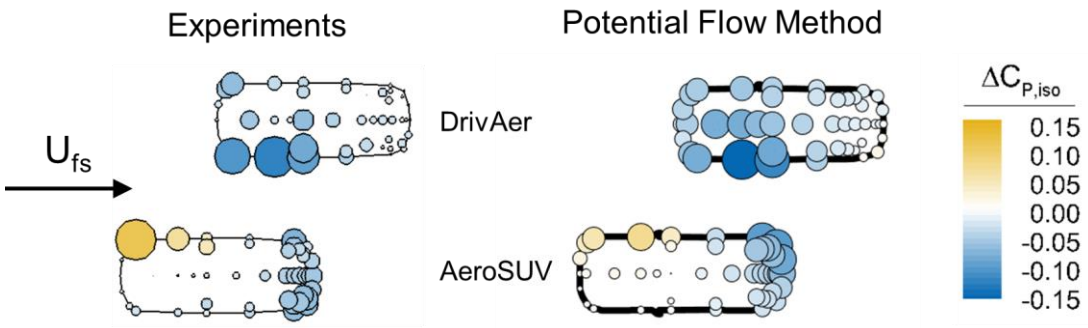

Figure 5: Top-down view comparing the experimental and predicted $\Delta C_{P,iso}$ changes due to proximity with adjacent-lane vehicles, at a half-vehicle-length offset. The Potential Flow Method shows values calculated at the pressure-tap locations.

To estimate the change in drag coefficient for each vehicle, an assumption is made that the incremental drag (ΔC_D) is proportional to the difference in incremental pressure (ΔC_P) across the longitudinal length of the vehicle. To do this, the ΔC_P field is interpolated onto rectangular planes, perpendicular to the freestream flow and located at the leading and trailing edges of the assumed vehicle shape, with a width and a height equivalent to those dimensions of the assumed vehicle shapes. The ΔC_P values within each interpolated plane are then area averaged, and the difference between the leading- and trailing-edge-plane values is calculated ($\Delta C_{P,l\text{-}t}$). This value is then assumed to be proportional to the ΔC_D of the vehicle.

Figure 6 compares the estimated ΔC_D values for both vehicle models, and for the combined two-vehicle system, with the corresponding experimental measurements that were made over a range of ±2 vehicle-length offsets. Negative x/L values represent the AeroSUV forward of the DrivAer. The calculated $\Delta C_{P,l\text{-}t}$ values are scaled by a factor 0.7 to provide the ΔC_D estimates for the potential- flow method. Good agreement is found for the trends of ΔC_D for each vehicle and for the combined system. The larger influence of the AeroSUV on the DrivAer, due to the size difference, is replicated well, as are the distances over which each body experiences drag increases versus drag decreases. As with the experimental measurements, the combined incremental drag is highest when side by side (x/L = 0) and show minima in the x/L=±1 to ±2 range.

These results are preliminary, and the potential-flow approach has not yet been validated for larger or smaller lateral offsets, for different vehicle lengths, or for cross winds. However, the results presented here show that the use of a simple and efficient potential-flow method can provide a reasonable estimation of proximity effects, and may provide a means to estimate sensitivity geometric changes for multi-vehicle (2 or more) and multi-lane systems (2 or more).

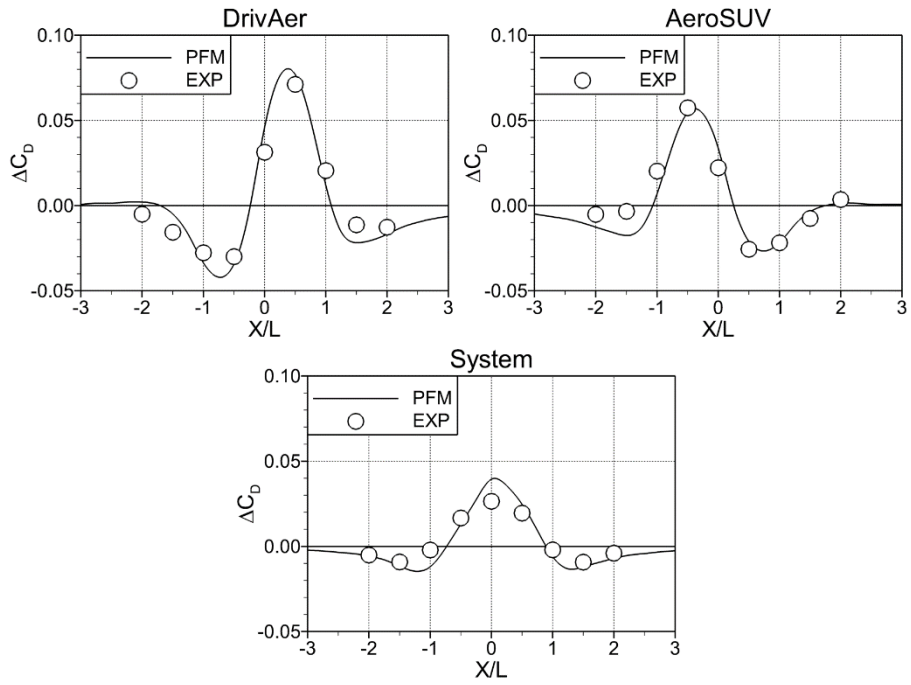

Figure 6: Comparison of drag-change-coefficient prediction using the potential-flow method (PFM) compared to experimental data (EXP) for the DrivAer Notchback and AeroSUV Estateback combination. Top plots show individual vehicles and bottom plot shows the two-vehicle system.

4 Conclusions

Mapping the aerodynamic performance of representative traffic scenarios typically requires extensive wind tunnel testing or prolonged on-road measurements. In this study, a low-order CFD simulation was employed to model interaction effects in proximity situations. In addition, a simplified and computationally efficient potential flow method was applied, producing results in alignment with experimental data. The findings demonstrate that these simplified and cost-effective methods can serve as effective tools for analyzing proximity interactions of traffic while reducing the expenses associated with purely experimental approaches. These methods show strong potential for the efficient estimation of proximity effects; however, further investigation is warranted, particularly to address crosswind conditions and variations in vehicle geometry.

5 Reference list

[1] Jessing, C., Wilhelmi, H., Wittmeier, F., Wagner, A. et al., “Investigation of Transient Aerodynamic Effects on Public Roads in Comparison to Individual

Driving Situations on a Test Site," SAE Technical Paper 2020-01-0670, 2020, doi:10.4271/2020-01-0670.

[2] Wang, Z., Bian, Y., Shladover, S.E., Wu, G., Li, S.E., Barth, M.J., 2019. "A survey on cooperative longitudinal motion control of multiple connected and automated vehicles." IEEE Intelligent Transportation Systems Magazine," doi:10.1109/MITS.2019.2953562.

[3] McAuliffe, B. and Barber, H., "Simulating Traffic-wake Effects in a Wind Tunnel," SAE Int. J. Advances & Curr. Prac. in Mobility 5(6):1969-1987, 2023, doi:10.4271/2023-01-0950.

[4] Dasarathan, D., He, W., Spencer, S., and Gargoloff, J., "Influence of Class-8 Truck Passing Oncoming Truck Using CFD Simulation," SAE Technical Paper 2022-01-1151, 2022, doi:10.4271/2022-01-1151.

[5] McAuliffe, B., Sowmianarayanan, B., and Barber, H., "Near-to-Far Wake Characteristics of Road Vehicles Part 1: Influence of Ground Motion and Vehicle Shape," SAE Int. J. Advances & Curr. Prac. in Mobility 3(4):2009-2024, 2021, doi:10.4271/2021-01-0957.

[6] Shimizu, K., Nakashima, T., Hiraoka, T., Nakamura, Y. et al., "Investigation of Increase in Aerodynamic Drag Caused by a Passing Vehicle," SAE Technical Paper 2018-01-0719, 2018, doi:10.4271/2018-01-0719.

[7] McAuliffe, B. and Barber, H., "Aerodynamic Drag of Road Vehicles in Close Lateral Proximity," SAE Int. J. Advances & Curr. Prac. in Mobility 5(6):2004-2020, 2023, doi:10.4271/2023-01-0952.

[8] McAuliffe, B. and Barber, H., "Wind-Load and Surface-Pressure Measurements of the Aerodynamic Interactions of a Passenger Vehicle with Adjacent-Lane Vehicles," SAE Technical Paper 2024-01-2549, 2024, doi:10.4271/2024-01-2549.

[9] Wickern, G., "On the Application of Classical Wind Tunnel Corrections for Automotive Bodies," SAE Technical Paper 2001-01-0633.

[10] Le Good, G., Self, M., Boardman, P., Resnick, M. "An Investigation of Aerodynamic Characteristics of Three Bluff Bodies in Close Longitudinal Proximity-Part 2," SAE Technical Paper 2021-01-0952, 2021, doi: 10.4271/2021-01-0952.

[11] Aultman, M., Wang, Z., Auza-Gutierrez, R., Duan, L., "Evaluation of CFD methodologies for prediction of flows around simplified and complex automotive models" Computers and Fluids, vol. 236, 2022, doi: 10.1016/j.compfluid.2021.105297.